DOI: 10.1002/chem.201000433

Two-Step Thermal Spin Transition and LIESST Relaxation of the Polymeric Spin-Crossover Compounds $Fe(X\text{-}py)_2[Ag(CN)_2]_2$ (X = H, 3-methyl, 4-methyl, 3,4-dimethyl, 3-Cl)**

J. Alberto Rodríguez-Velamazán,*[a] Chiara Carbonera,[a, b] Miguel Castro,[a] Elías Palacios,[a] Takafumi Kitazawa,[c] Jean-François Létard,[b] and Ramón Burriel[a]

Abstract: In the series of polymeric spin-crossover compounds $Fe(X\text{-}py)_2[Ag(CN)_2)]_2$ (py = pyridine, X = H, 3-Cl, 3-methyl, 4-methyl, 3,4-dimethyl), magnetic and calorimetric measurements have revealed that the conversion from the high-spin (HS) to the low-spin (LS) state occurs by two-step transitions for three out of five members of the family (X = H, 4-methyl, and X = 3,4-dimethyl). The two other compounds (X = 3-Cl and 3-methyl) show respectively an incomplete spin transition and no transition at all, the latter remaining in the HS state in the whole temperature range. The spin-crossover behaviour of the compound undergoing two-step transitions is well described by a thermodynamic model that considers both steps. Calculations with this model show low cooperativity in this type of systems. Reflectivity and photomagnetic experiments reveal that all of the compounds except that with X = 3-methyl undergo light-induced excited spin state trapping (LIESST) at low temperatures. Isothermal HS-to-LS relaxation curves at different temperatures support the low-cooperativity character by following an exponential decay law, although in the thermally activated regime and for aX = H and X = 3,4-dimethyl the behaviour is well described by a double exponential function in accordance with the two-step thermal spin transition. The thermodynamic parameters determined from this isothermal analysis were used for simulation of thermal relaxation curves, which nicely reproduce the experimental data.

Keywords: calorimetry · iron · magnetic properties · spin crossover

Introduction

Materials that undergo variation of their physical properties under external perturbations such as temperature, light, pressure, and electric and magnetic fields are potential candidates for applications in information storage devices, molecular switches and sensors. Spin-crossover (SCO) compounds, most commonly Fe^{II} complexes, in which the spin state of the transition metal can be switched in a controlled manner between low-spin (LS) and high-spin (HS) states, belong to this class of materials.[1,2]

Interaction with light has attracted much attention following the discovery of light-induced excited spin state trapping (LIESST) in 1984.[3] Irradiation of an SCO compound at low temperature with precise wavelengths induces formation a metastable HS state from the LS state. The latter can be subsequently recovered either by the reverse LIESST effect, which occurs if irradiation at a different wavelength is performed, or by thermal relaxation if the temperature of the sample is sufficiently increased. Since the latter process depends on the heating rate, a characteristic temperature,[4] denoted T(LIESST), has been experimentally defined to describe the stability of the induced HS state. A systematic study has shown a correlation between the temperature corresponding to the HS–LS thermal transition $T_{1/2}$ and T(LIESST), which is estimated from the maxima of the $d(\chi T)/dT$ curve, where χ is the magnetic susceptibility and T the temperature.[4]

[a] Dr. J. A. Rodríguez-Velamazán, Dr. C. Carbonera, Dr. M. Castro, Dr. E. Palacios, Prof. Dr. R. Burriel
Instituto de Ciencia de Materiales de Aragón (ICMA)
CSIC - Universidad de Zaragoza, 50009 Zaragoza (Spain)
E-mail: jarv@unizar.es

[b] Dr. C. Carbonera, Prof. Dr. J.-F. Létard
Laboratoire des Sciences Moléculaires
Institut de Chimie de la Matière Condensée de Bordeaux (ICMCB)
CNRS UPR No 9048, 33608 Pessac (France)

[c] Prof. Dr. T. Kitazawa
Department of Chemistry, Faculty of Science, Toho University
Miyama, Funabashi, Chiba, 274-8510 (Japan)

[**] LIESST: light-induced excited spin state trapping.

Strong intermolecular interactions between SCO metal centres give rise to a cooperative behaviour affecting significantly the thermal spin transition (increasing its abruptness and hysteresis), the LIESST effect and the relaxation process. One of the routes for the cooperativity enhancement is the polymeric approach,[5] in which the switching sites are linked by chemical bridges into extended or polymeric structures with varying dimensionality and topology.[6] The number of polymeric compounds in which the LIESST effect has been studied is rather small compared with other types of spin-crossover compounds.[7,8]

Along this approach, Hofmann-like SCO clathrate polymeric compounds, in which the metal centres are linked with cyanometallate complexes, have been intensively investigated. The first such compound, $Fe(py)_2[Ni(CN)_4]$ (py = pyridine), synthesised by Kitazawa et al. in 1996,[9] shows a two dimensional (2D) structure and a cooperative spin transition. Substitutions in the py ligand[10] give rise to different magnetic behaviours including incomplete gradual or cooperative transitions and even two-step spin transitions induced by pressure.[11,12] The LIESST effect has not been reported for these compounds.

The use of different ligands and cyanide complexes gives rise to 2D and 3D interpenetrated networks and architectural isomerism with different magnetic behaviours. For example, the 2D compound $Fe(pmd)_2[Cu(CN)_2]_2$ (pmd = pyrimidine)[7e] undergoes both a complete cooperative thermal spin transition at around 140 K and LIESST conversion (T(LIESST) = 73 K). If Ag is used instead of Cu, two 3D polymorphs of $Fe(pmd)_2[Ag(CN)_2]_2$ are obtained,[13] and a 3D topology is also obtained for $Fe(3\text{-}CNpy)_2[M(CN)_2]_2 \cdot n H_2O$ (M = Ag, Au),[14] which exist as three supramolecular isomers showing different magnetic behaviours. To our knowledge, photomagnetic studies have not been performed on these systems. In contrast, interesting photoswitching around room temperature between LS and HS state has been induced by a laser pulse in the hysteresis loop of the thermal spin transition for the Pt compound[15] of the 3D polymeric family $Fe(pz)_2[M(CN)_4] \cdot n H_2O$ (pz = pyrazine; M = Ni, Pd, Pt).[16] Moreover, compounds $[Fe(azpy)[M(CN)_4] \cdot n H_2O$ (azpy = 4,4′-azopyridine; M = Ni, Pd, Pt) have been reported[17] as polycrystalline bulk samples and thin films on gold substrates. They show a 3D structure and spin transitions above 150 K depending on the transition metal ion and on the water content. The LIESST effect was also detected (but not deeply studied) in all of them except for the powder sample with M = Ni.

High structural complexity is attained by the $\{Fe(pmd)[Ag(CN)_2)][Ag_2(CN)_3]\}$[7d] system with a self-interpenetrated 3D polymeric structure showing a two-step spin transition and photomagnetic behaviour explained by the presence of five crystallographically different iron atoms. The bimetallic doubly interpenetrated 3D complexes $[Fe(L)_x[Ag(CN)_2]_2] \cdot G$ show LS and HS states in the whole temperature range for L = pz ($x = 1$, G = pz) and L = 4,4'-bipyridine ($x = 2$), respectively. However, for L = bispyridylethylene ($x = 2$), a strong cooperative spin transition with a hysteresis of 95 K and a T(LIESST) of about 71 K are detected.[18]

Recently, we reported the 2D polymeric spin-crossover compound $Fe(py)_2[Ag(CN)_2]_2$,[19] which undergoes a two-step spin transition. Powder X-ray diffraction data and Mössbauer spectroscopy revealed the existence of only one Fe^{II} site at room temperature and that, on lowering temperature, no crystallographic phase transition accompanies the two-step spin transition. However, a large increase of the average thermal factor at the plateau is detected and seems to be compatible with a disordered distribution of spin states.

Halogen substitution of the last-named type of compound gave $Fe(3\text{-}Xpy)_2[M(CN)_2]_2$ (X = F, Cl, Br, I; M = Ag, Au),[20,21] which show similar structures constituted of stacks of 2D coordination polymers organised in pairs. All of the gold derivatives are HS in the whole temperature range, except for that with 3-Fpy, which undergoes a half-spin transition around 140 K with a small hysteresis of 5 K, although under pressure (0.18–0.26 GPa) it undergoes a complete two-step spin transition. Additionally, a structural transition accompanying the thermal spin transition creates two crystallographically independent Fe^{II} sites. In the case of the silver compounds, only those with 3Fpy and 3Clpy show a spin transition. For the former, a low-cooperative two-step transition takes place, with $T_{1/2}$(step 1) = 162 K and $T_{1/2}$(step 2) = 96 K (due to the presence of two crystallographically distinct Fe^{II} sites), and an incomplete transition at $T_{1/2} = 106$ K (only one Fe^{II} site and 50% conversion) is shown by the latter. However, the 3Brpy and 3Ipy derivatives remain in the HS state in the whole temperature range. The expected decrease of the ligand field (and therefore decrease of $T_{1/2}$) as the electronegativity of the ligand Xpy increases has not been observed, and the behaviour can be explained considering attenuation of the lattice pressure as the polarisability of the halogen atom is higher. The LIESST effect has not been studied.

Here we report magnetic, photomagnetic, calorimetric, Mössbauer and reflectivity studies on $Fe(X\text{-}py)_2[Ag(CN)_2)]_2$ (X = H, 3-Me, 4-Me, 3,4-Me_2, 3-Cl, where the numbers indicate the substitution position in the pyridine ring). The influence on the SCO behaviour of the substitutions in the py ligand is discussed and compared with the parent and halogen-substituted compounds. The main distinctive property of this family is the presence of two-step transitions in most of the compounds. Moreover, the members of the family characterised by a two-step thermal spin transition also reveal a two-step character in the relaxation of the photoinduced HS metastable state, which is a very rare feature in mononuclear systems.

Results and Discussion

Magnetic properties: The magnetic behaviour of $Fe(X\text{-}py)_2[Ag(CN)_2]_2$, shown in Figure 1, depends significantly on the substituents of the pyridine ligand. As previously report-

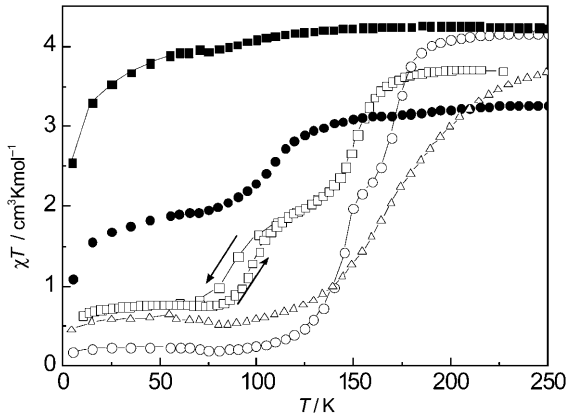

Figure 1. Temperature dependence (on cooling, except for **X=H** for which heating and cooling curves are displayed) of χT for Fe(X-py)$_2$[Ag(CN)$_2$]$_2$: (□) **X=H**; (●) **X=3-Cl**; (■) **X=3-Me**; (△) **X=4-Me**; (○) X=**X=3,4-Me$_2$**.

ed,[19] for **X=H** spin conversion occurs in two steps. At high temperature, the χT product is 3.66 cm^{3}K mol^{-1}, in agreement with the expected value for the HS state of an Fe^{2+} ion. As the temperature decreases, χT remains constant until 190 K, and then undergoes a large decrease to 2.25 cm^{3}K mol^{-1} at 140 K (step 1). Between 140 and 110 K, χT shows a small plateau, and below 110 K, it finally falls, reaching a value which depends on the cooling rate (step 2), since trapping of HS species at low temperature occurs.[19] For a slow cooling rate (0.35 K min^{-1}) χT is 0.75 cm^{3}K mol^{-1} at 60 K. This value corresponds to a residual fraction of around 23% of HS species which undergo zero-field splitting, and therefore a decrease of the magnetic moment at low temperature is observed. The subsequent heating measurement (1 K min^{-1}) shows thermal hysteresis for step 2. Transition temperatures are $T_{1/2,1}=146$ K for the high-temperature step and $T_{1/2,2\uparrow}=98$ K (on heating) for the low-temperature step. For this second step, the transition temperature on cooling depends on the cooling rate, being $T_{1/2,2\downarrow}=$ 84 K at 0.35 K min^{-1}. For this low scan rate the spin conversion at steps 1 and 2 corresponds to 45 and 32% of the Fe^{II} centres, respectively. However, rapid cooling of the sample from 250 K induces considerable trapping of a metastable HS state at low temperature. The maximum amount of trapped species obtained by the fastest cooling rate reached by the instrument (10 K min^{-1}) is equal to that involved in the second step. The halogen substituted compound **X=3-F** shows a similar two-step process regarding the transition temperatures, but without hysteresis.[20]

When a methyl group substitutes a hydrogen atom on the pyridine ligand, a drastic change in the magnetic behaviour is produced. Depending on the substitution position, spin conversion can be completely suppressed, as for **X=3-Me**, which remains in the HS state in the whole temperature range. However, a small anomaly appears at about 75 K which may be symptomatic of incomplete SCO. The same behaviour has been reported for the halogen-substituted compounds **X=3-Br** and **X=3-I**, which also maintain the HS state.[20]

In contrast, for **X=4-Me**, the LS state seems to be favoured, since the compound undergoes a gradual spin conversion, centred at about 175 K, over a broad temperature range of more than 150 K. In this last case, a residual paramagnetism of $\chi T \approx 0.5$ cm^{3}K mol^{-1} is observed below 90 K.

However, the substitution of two hydrogen atoms by methyl groups (**X=3,4-Me$_2$**) leads to the recovery of a clear two-step behaviour and also a small decrease in the average of the transition temperatures. In this case, the high-temperature value of χT is 4.20 cm^{3}K mol^{-1} as for **X=3-Me**. At 200 K, the spin transition starts and covers a temperature range of around 90 K with a plateau at around 160 K. This transition is markedly more abrupt than in the case of **X=H**, but the process does not show any thermal hysteresis. The transition temperatures are $T_{1/2,1}=171$ K and $T_{1/2,2}=$ 145 K for the high- and low temperature step, respectively. Around 47% of spin conversion is produced in step 1, and 53% in step 2. The residual paramagnetism at low temperature is in this case lower than for **X=4-Me**, with a value of around 0.2 cm^{3}K mol^{-1} indicating the practical absence of a residual fraction of HS species, as confirmed by Mössbauer results (see below).

For **X=3-Cl** an incomplete spin transition is detected, in agreement with the work of Real et al.[20] The value of χT decreases very slowly from 3.3 cm^{3}K mol^{-1} at high temperature to 3.05 cm^{3}K mol^{-1} at 140 K, where a gradual spin transition starts. At 60 K, a value of 1.9 cm^{3}K mol^{-1} is reached, corresponding to about 40% spin conversion. The decrease in magnetic moment at low temperature can be attributed to the zero-field splitting of the residual fraction of around 60% of HS species. The transition temperature $T_{1/2}=109$ K is slightly higher than the previously reported value (106 K) and the transition in our compound is less abrupt. These differences may be related to the quality and size of the crystals.

Considering the electronic effect due to the substitution within the ligand, it is expected that a decrease in the ligand field and in the $T_{1/2}$ value should be induced as the electronegativity of the ligand increases.[22,23] For the halogen-substituted compounds, however, the opposite tendency is observed, as the HS state is stabilised with increasing size of the halogen atoms.[20] The more efficient attenuation of the internal pressure of the lattice (and therefore of the ligand field strength felt by the Fe^{II} ions) when highly polarizable atoms are present in the crystal is invoked as a possible explanation for the trend of $T_{1/2}$ in these halogen-substituted compounds. If we compare the compounds **X=3-Cl** and **X=3-Me** of our series, taking into account the fact that the electronegativity of the methyl group is much lower than that of Cl, the same trend as in the series of halogen-substituted compounds seems to be present. However, when comparing **X=3-Cl** and **X=4-Me**, the contrary is observed. The lack of precise structural information on our series prevents our giving the type of explanation cited for the halogen-substituted compounds, but it seems that the position of the

substituent must play an important role, perhaps by inducing steric effects and inter-ligand interactions, which produce completely different magnetic behaviours.

^{57}Fe Mössbauer spectroscopy: Mössbauer spectra for all compounds are shown in Figure 2. The parameters coming from the fits and the calculated HS and LS fractions are listed in Table 1.

In accordance with the magnetic susceptibility, the Mössbauer spectra reveal that **X = 3-Me** (Figure 2a) remains in the HS state at both temperatures. The Mössbauer data of **X = H**, reported previously, are also in agreement with the magnetic data,[19] and the spectra do not show any evidence of the existence of two different Fe^{II} sites that could be at the origin of the two-step behaviour.

Compound **X = 4-Me** was studied at different temperatures between 290 and 77 K (Figure 2b). The spectra were analysed with a doublet for the HS site and a singlet for the LS site. At temperatures where HS and LS species coexist, the fit was done by considering the same width σ_{exp} for both lines of the HS doublet, while at high temperature, a different σ_{exp} is considered for each line. Isomer shifts (IS) are given relative to α-Fe at room temperature. The data of the HS fraction were obtained by assuming identical Mössbauer–Lamb factors for HS and LS states. At room temperature, the system is in the HS state. On lowering the temperature, coexistence of HS and LS species is observed, with a continuous decrease of the HS species. Finally, for $T < 90$ K, all the Fe^{II} centres are in the LS state, with no evidence of paramagnetic residue. The residual paramagnetism at low temperatures shown by the magnetic measurements could be explained by slight differences in synthesis of different samples.

In the case of **X = 3,4-Me$_2$** (Figure 2c) the data indicate 100% HS species at room temperature and 100% LS species at 77 K, as is expected in accordance with the magnetic data, which show that only a small paramagnetic contribution still exists at low temperature. Finally, for **X = 3-Cl** (Figure 2d) a decrease of the HS fraction, from 100% at 290 K

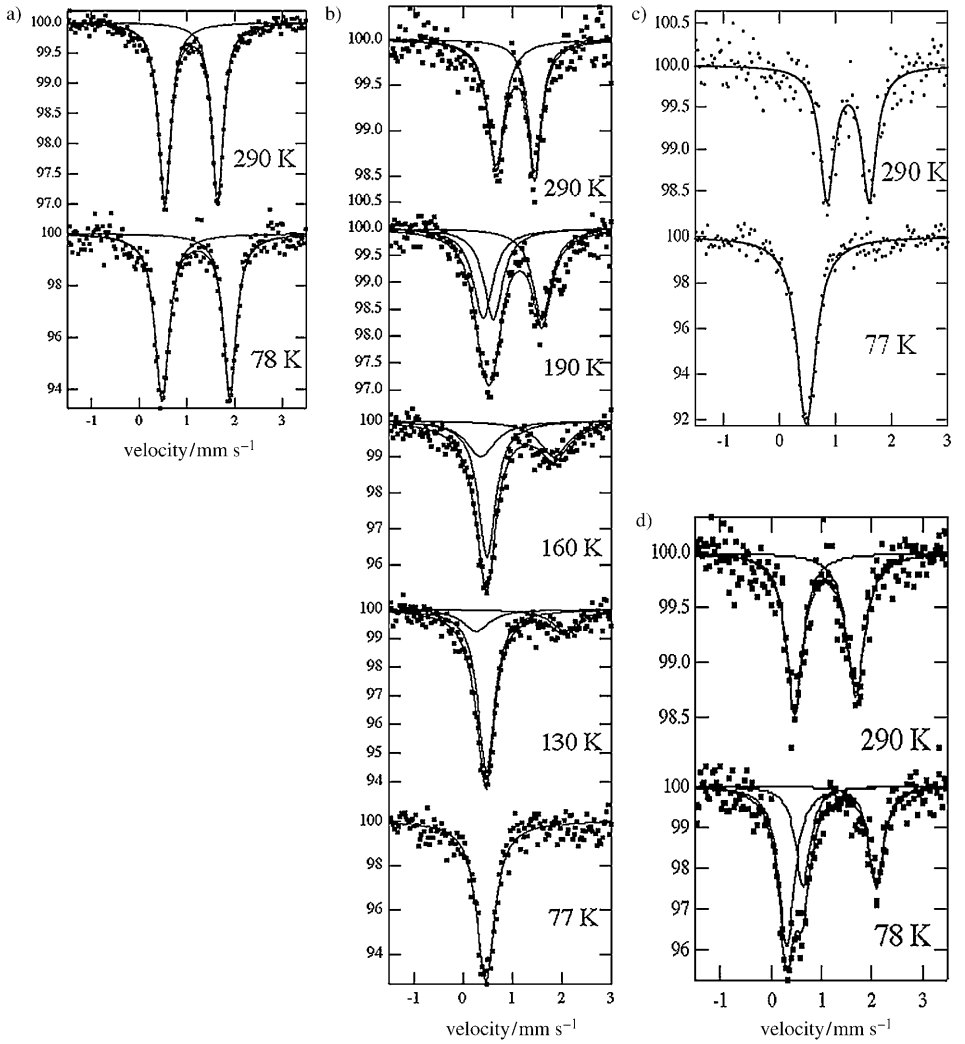

Figure 2. Mössbauer spectra of a) **X = 3-Me**, b) **X = 4-Me**, c) **X = 3,4-Me$_2$** and d) **X = 3-Cl**. Vertical axis: relative intensity (%).

Table 1. Mössbauer parameters (I.S.: isomer shift, Q.S.; quadrupole splitting, σ_{exp}: peak width) and area fractions of the characteristic subspectra corresponding to the HS state for $Fe(X\text{-}py)_2[Ag(CN)_2]_2$ at selected temperatures.

X	T [K]	Site	I.S. [mm s^{-1}]	Q.S. [mm s^{-1}]	σ_{exp} [mm s^{-1}]	Area fraction [%]
3-Me	290	HS	1.09	1.10	0.30/0.29	100
	78	HS	1.19	1.42	0.35/0.32	100
4-Me	290	HS	1.06	0.78	0.41/0.33	100
	190	HS	1.10	0.99	0.46	65.9
		LS	0.41		0.49	34.1
	160	HS	1.10	1.48	0.73	47.1
		LS	0.48		0.42	52.9
	130	HS	1.16	1.80	0.65	30.1
		LS	0.47		0.40	69.9
	77	LS	0.46		0.44	0
3-Cl	290	HS	1.07	1.21	0.39/0.43	100
	78	HS	1.36	1.45	0.35	53.5 (30)
		LS	0.31		0.38	46.5 (30)
3,4-Me$_2$	290	HS	1.23	0.75	0.32/0.32	100
	77	LS	0.64		0.41	100

to 53.5% at 78 K, was determined, also in agreement with the magnetic measurements.

Heat capacity: Heat capacity data are shown in Figure 3. The heat capacity measurements on **X = 3-Me** (not shown) did not reveal any anomaly in the whole temperature range, in accordance with its permanent HS state. For the other compounds, in order to evaluate the enthalpy (ΔH) and entropy (ΔS) variations, a non-anomalous contribution was estimated by using a smooth function interpolated from the heat capacity values out of the spin-transition region and finally subtracted. For **X = 4-Me**, the data show two overlapping peaks with maxima at $T_{c1} = 189$ K and $T_{c2} = 147.5$ K. Although, in the absence of precise structural information, we cannot discard other origins for the high temperature peak, such as methyl-group rotation, the calorimetric measurements—in contrast with other characterisation techniques–most likely reveal a two-step spin transition, as also observed in **X = H** and **X = 3,4-Me$_2$** (see below). The overall ΔH and ΔS are 10.8 kJ mol^{-1} and 64.7 J mol^{-1} K^{-1}, respectively, and the values are within the experimental range generally observed for Fe^{II} SCO compounds.[24] In order to estimate from these overlapped peaks the enthalpy and entropy contents associated with each step, the anomalous heat capacity was fitted to the sum of two Lorentzian functions. Thus, the thermodynamic quantities associated with each step are $\Delta H_1 = 5.5$ kJ mol^{-1}, $\Delta S_1 = 28.6$ J mol^{-1} K^{-1}; $\Delta H_2 = 5.3$ kJ mol^{-1}, $\Delta S_2 = 36.1$ J mol^{-1} K^{-1}.

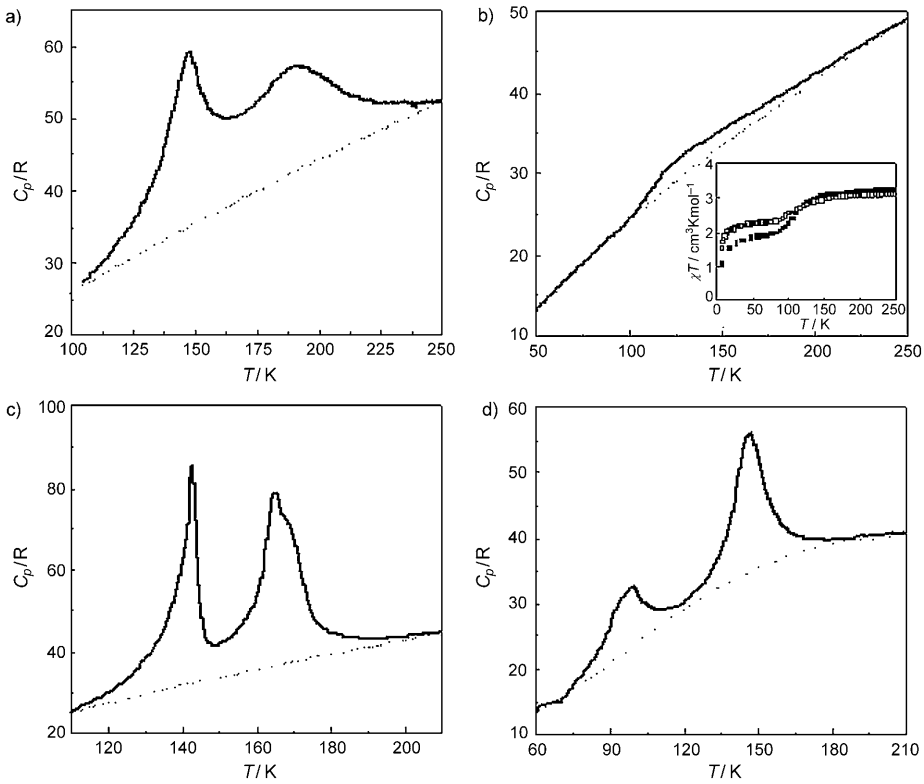

Figure 3. Heat capacity data for $Fe(X\text{-}py)_2[Ag(CN)_2]_2$: The estimated non-anomalous contribution is represented as a dotted line for each compound. a) **X = 4-Me** (DSC), b) **X = 3,4-Me$_2$** (DSC), c) **X = 3-Cl** (AC calorimetry). Inset: Magnetic behaviour of a pellet sample (□) compared with a powder one (■). d) **X = H** (Adiabatic calorimetry, taken from ref. [19]).

The heat capacity curve of compound **X = 3,4-Me$_2$**, obtained by differential scanning calorimetry (DSC), also shows two asymmetrical and well-separated anomalies associated with the two steps of the transition. The peak corresponding to step 1 is centred at $T_{c1} = 165$ K and shows a shoulder on its high-temperature side, while for step 2 a sharper peak is observed with maximum at $T_{c2} = 142.5$ K. The transition temperatures are slightly lower than those observed by magnetic susceptibility measurements. This difference is usually observed between magnetic and DSC results,[25] and can be attributed to the different scan rates in the two techniques (0.5 K min^{-1} on cooling in magnetic measurements and 10 K min^{-1} in DSC). Considering the limit between the two steps at 150 K, the enthalpy and entropy values associated with each step are $\Delta H_1 = 5.6$ kJ mol^{-1}, $\Delta S_1 = 32.2$ J mol^{-1} K^{-1}; $\Delta H_2 = 3.2$ kJ mol^{-1}, $\Delta S_2 = 25.5$ J mol^{-1} K^{-1}. A different change in entropy is observed between step 1 and step 2 in these two last compounds that, considering precedents in the literature,[7d] could be due to variation of unit-cell volume between the two steps. Unfortunately, single crystals could not be obtained from these compounds, and the structures could not be resolved from powder X-ray diffraction measurements, which makes it unwise to make further conjectures about structural aspects.

Calorimetric measurements on compound **X = 3-Cl** were performed by AC calorimetry, in order to have access to lower temperatures than with DSC (Figure 3c). The heat capacity curve shows a small and broad anomaly with maximum around 120 K. The thermodynamic quantities associated with the transition ($\Delta H = 1.33$ kJ mol^{-1} and $\Delta S = 8.3$ J mol^{-1} K^{-1}) are much lower than those observed for the other compounds of the family. However, in this case the spin transition is incomplete and, as is shown in the inset of Figure 3c, the uniaxial pressure required to form a pellet for the AC measurements reduces the number of SCO centres that undergo the spin transition.[26] Taking into account this reduction, the estimated enthalpy and entropy values would be $\Delta H \approx 2.5$ kJ mol^{-1} and $\Delta S \approx 15$ J mol^{-1} K^{-1} and finally, considering the incompleteness of the transition described in the magnetic measurements (40% of spin conversion), $\Delta H \approx 6.25$ kJ mol^{-1} and $\Delta S \approx 37.55$ J mol^{-1} K^{-1} per mole which undergoes the spin-crossover transition.

A thermodynamic study on compound **X = H** was reported elsewhere, but the results are also shown in Figure 3 for comparison.[19] The enthalpy and entropy contents associated with the two steps of transition were $\Delta H_1 = 3.33\ \mathrm{kJ\,mol^{-1}}$, $\Delta S_1 = 22.6\ \mathrm{J\,mol^{-1}\,K^{-1}}$; $\Delta H_2 = 1.51\ \mathrm{kJ\,mol^{-1}}$ and $\Delta S_2 = 15.7\ \mathrm{J\,mol^{-1}\,K^{-1}}$. The entropy contents are typical values for SCO compounds.[24]

The consistency of the thermodynamic and magnetic data can be analysed using a simple model proposed by Real et al.,[7d] based on the regular solution model of Slichter and Drickamer.[27] Additionally, this model gives information about the cooperativity of these compounds. The model considers two independent groups of SCO centres that undergo the spin transition at two different temperatures. The total high spin fraction can be written as Equation (1),

$$\gamma_{HS} = (1-c)\gamma_{HS1} + c\gamma_{HS2} \quad (1)$$

where $\gamma_{HS1,2}$ are the high-spin fractions for each step, both of which range from 0 to 1, and c is the value of γ_{HS} in the plateau. The cooperativeness is included by means of four phenomenological interaction constants introduced in the expression of the Gibbs free energy: Γ_{11}, Γ_{22} for the interaction within the groups, and Γ_{12}, Γ_{21} for the interaction between the two groups. The system of coupled Equations (2) thus describes the two-step spin transition,

$$\ln\left[\frac{1-\gamma_{HS1}}{\gamma_{HS1}}\right] = \frac{[\Delta H_1 + \Gamma_{11}(1-2\gamma_{HS1}) - 2\Gamma_{12}\gamma_{HS2} - T\Delta S_1]}{RT} \quad (2a)$$

$$\ln\left[\frac{1-\gamma_{HS2}}{\gamma_{HS2}}\right] = \frac{[\Delta H_2 + \Gamma_{22}(1-2\gamma_{HS2}) - 2\Gamma_{21}(\gamma_{HS1}-1) - T\Delta S_2]}{RT} \quad (2b)$$

where $\Delta H_{1,2}$ and $\Delta S_{1,2}$ are respectively the enthalpy and entropy variations for the two groups, which are related to the experimental values by Equations (3) and (4)

$$\Delta H_1(\gamma_{HS1} = 1/2;\ \gamma_{HS2} = 1) = \Delta H_1^{exp}/(1-c) \quad (3a)$$

$$\Delta H_2(\gamma_{HS1} = 0;\ \gamma_{HS2} = 1/2) = \Delta H_2^{exp}/c \quad (3b)$$

$$\Delta S_1 = \Delta S_1^{exp}/(1-c) \quad (4a)$$

$$\Delta S_2 = \Delta S_2^{exp}/c \quad (4b)$$

This system of coupled equations was solved numerically by optimising Γ_{11} and Γ_{22} and using the experimental values of $\Delta H_{1,2}$ and $\Delta S_{1,2}$ for each compound. Considering the hypothesis $\Gamma_{12} = \Gamma_{21}$ allows the number of parameters to be reduced. The results for all compounds which undergo the spin transition are presented in Figure 4, and compared with the experimental high-spin fraction obtained form the magnetic measurements.[28]

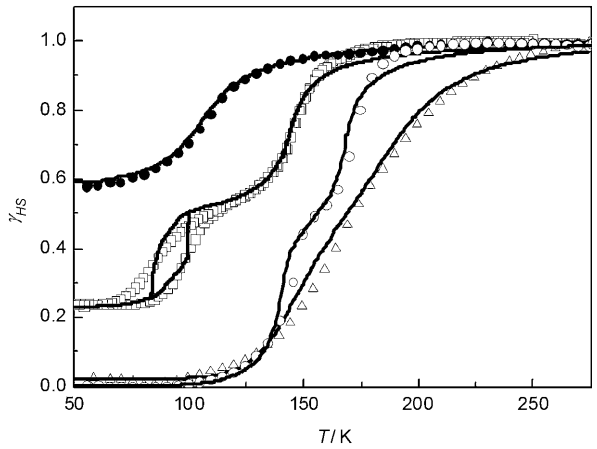

Figure 4. Temperature dependence of γ_{HS} deduced from the magnetic susceptibility measurements for $Fe(X\text{-}py)_2[Ag(CN)_2]_2$: **X = H** (□); **X = 3-Cl** (●); **X = 4-Me** (△); **X = 3,4-Me$_2$** (○), and simulation (continuous lines) as described in the text.

Despite its simplicity, the model allows the main features of the spin transitions of this family of compounds to be reproduced. For **X = H**, a residual fraction $r_{HS} = 0.23$ of SCO centres which remain in the HS state at low temperature was additionally considered, and the experimental enthalpy and entropy contents of steps 1 and 2 were taken to correspond to 47 and 30% of spin conversion, respectively, in accordance with the magnetic measurements. The calculation is insensitive to the value of Γ_{12}, due to the considerable difference in the transition temperatures of the two steps.[7d] The interaction constant within the first group which gives the best accordance with the magnetic data is $\Gamma_{11} = 1.9\ \mathrm{kJ\,mol^{-1}}$, and then $\Gamma_{11}/2RT_{c1} = 0.78 < 1$, as expected for a continuous process (without hysteresis).[27] The best agreement with the experimental results was obtained by considering a linear dependence of Γ_{22} on temperature, as proposed by Purcell and Edwards.[29] The optimised value is $\Gamma_{22}(T) = 0.135 + 0.016\,T\ \mathrm{kJ\,mol^{-1}}$, and then, $\Gamma_{22}(T_{c2})/2RT_{c2} = 1.05$ gives a hysteresis of 13 K, in accordance with the experimental data. Several factors can explain the discrepancy between the experimental and calculated curves, especially in the hysteresis-loop region. Firstly, the distribution of some of the parameters governing the SCO (energy barrier and difference in metal–ligand bond length Δr between the two states, etc.).[12] On the other hand, the differences may also have a kinetic origin: due to the slow HS–LS relaxation, the cooling branch (where the bigger discrepancies are observed) is extended over a wider temperature range for increasing scan rates.[19]

The proposed model can also reproduce the magnetic behaviour of compound **X = 4-Me**. In this case, c was considered to be equal to 0.5, in the absence of experimental evidences which would allow its value to be established more precisely, and $r_{HS} = 0$, in accordance with the Mössbauer results. The simulation is insensitive to Γ_{12}, the optimised interaction constants are $\Gamma_{11} = 1.1\ \mathrm{kJ\,mol^{-1}}$, $\Gamma_{22} = 0.5\ \mathrm{kJ\,mol^{-1}}$ and thus $\Gamma_{11}/2RT_{c1} = 0.35$, $\Gamma_{22}/2RT_{c2} = 0.21$. Both values are

much lower than unity, lie in the range of the lowest reported[30] and indicate poorly cooperative behaviour.

The simulation for compound **X = 3,4-Me$_2$** was performed by considering $r_{HS}=0$ and $c=0.53$, in accordance with the magnetic susceptibility and Mössbauer data. The optimised interaction constants within the groups are $\Gamma_{11}=2.3\ kJ\,mol^{-1}$ (i.e., $\Gamma_{11}/2RT_{c1}=0.84$) and $\Gamma_{22}=2\ kJ\,mol^{-1}$ (i.e., $\Gamma_{22}/2RT_{c2}=0.84$). These values, close to unity, explain the abruptness of both steps, although they are not large enough to produce hysteresis.

The gradual and incomplete spin transition of compound **X = 3-Cl** can be analysed by using the simple regular solution model,[27] considering $r_{HS}=0.58$. The interaction constant which better reproduces the experimental results is $\Gamma=1.0\ kJ\,mol^{-1}$, and then $\Gamma/2RT_c=0.55$ corresponds to a low-cooperativity system.

Optical properties: To obtain an indication of the possibility of photomagnetic properties in this family of compound, absorbance and reflectivity measurements were performed. In studies of absorbance versus wavelength at different temperatures, two main absorption bands are observed, at about 540 and 830 nm, for all the members of the family. These bands could be attributed to the $^1A_1\rightarrow{}^1T_1$ and $^5T_2\rightarrow{}^5E$ transitions.[31] The former grows with increasing LS fraction, and the latter with increasing HS population. Figure 5a shows the behaviour of compound **X = 4-Me**, as an example of such kind of measurements.

The reflectivity as a function of temperature at $\lambda=532$ nm for all compounds is also shown in Figure 5. All members of this family (with one exception, i.e., **X = 3-Me**, which does not show SCO) exhibit responsive behaviour and some common features. At high temperature, thermal spin transition is observed, while in the low-temperature region the measurements reveal a quantitative photo-induction corresponding to a light-induced thermal hysteresis (LITH) process.[32]

The temperature dependence of the reflected intensity at 532 nm for **X = H** is plotted for the cooling and heating modes in Figure 5b. A two-step thermal transition with hysteresis in step 2 was determined, in agreement with the magnetic data. Below 85 K the signal increases, that is, a photo-induced process converting LS to HS state is activated, and LITH is observed. The relative amplitude of step 2 is smaller than in the magnetic curve. This is seemingly related, on the one hand, with the higher scan rate in the reflectivity measurements (ca. 13 and ca. 10 K min^{-1} for cooling and heating, respectively, in the range 50–150 K), which causes significant trapping of the SCO centres in HS due to rapid cooling. On the other hand, continuous irradiation in this temperature range favours the HS state and therefore goes in the same direction.

The spectra of **X = 3-Me** are qualitatively similar to those shown in Figure 5a, although the absorbance of the sample is globally smaller. Notwithstanding, a non-negligible effect in the range 75–100 K is noticeable when we plot the intensity of the band centred at 532 nm as function of temperature (Figure 5c).

In the dimethylated complex (**X = 3,4-Me$_2$**), two abrupt thermal transition steps are clearly evident (Figure 5c), in agreement with the magnetic and calorimetric data. In contrast, the reflectivity curve in the thermal transition range for **X = 4-Me** (Figure 5d) is analogous to the magnetic susceptibility curve and the presence of a two-step SCO is not evident. In the low-temperature region, we observe photo-induction of the HS state, with LITH effect starting below 60 K for the latter compound and below 75 K for the former.

Finally, the reflectivity at $\lambda=$ 532 nm of **X = 3-Cl** (Figure 5d) shows, in accordance with the magnetic data, a gradual and incomplete HS-to-LS transition between 200 and 80 K. Below this temperature, irradiation produces almost complete return to the HS state and, as in the previous compounds, the LITH effect is observed.

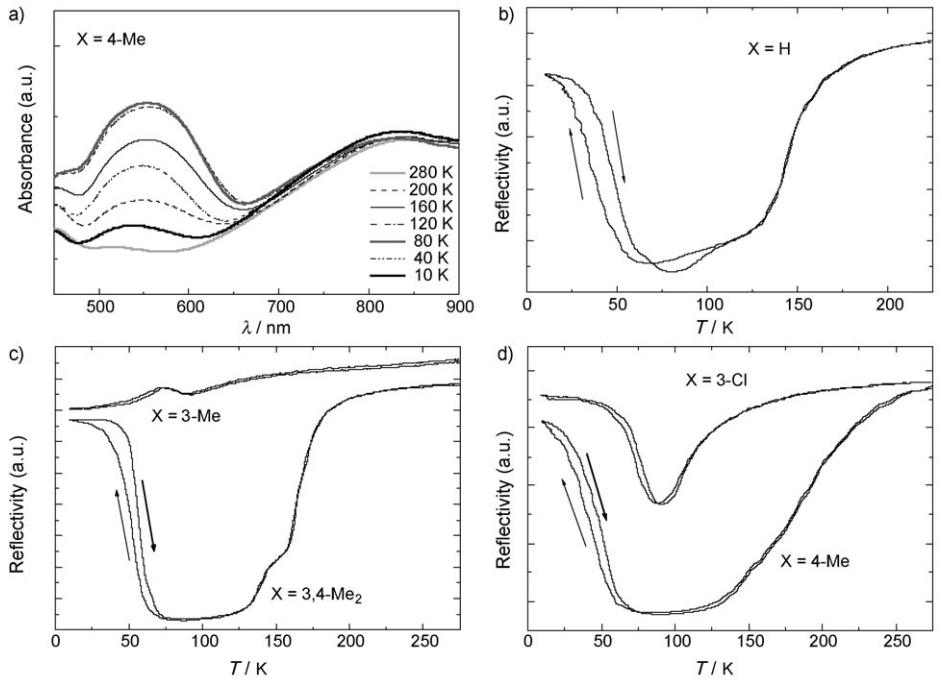

Figure 5. Reflectivity measurements on Fe(X-py)$_2$[Ag(CN)$_2$]$_2$. a) Absorbance spectra of **X = 4-Me** at different temperatures. b–d) Reflectivity as a function of temperature at 532 ± 2.5 nm for all compounds.

LIESST effect: The photo-magnetic properties of the compounds that present a thermal spin transition were investigated by the *T*(LIESST) procedure.[4] Briefly, the sample is irradiated for a variable duration

of time (on the order of 1–2 h) with laser light at 530.9 nm. Once the photostationary point was reached, the light was switched off and the susceptibility measured as a function of the temperature on heating from 10 to 300 K. The *T*-(LIESST) value was established at the point of maximum slope of the LIESST curve.

The photomagnetic curves shown in Figure 6 prove that under suitable irradiation quantitative photoconversion of the LS to the metastable HS form of the complexes is reached in all cases. It is noteworthy that the photoinduced HS fraction strongly depends on the intensity of the light. Moreover, in the cases where a two-step SCO occurs, a threshold effect between 50% and complete photoexcitation is observed. That is, when the power is around 2 mW cm^{-2}, whatever the irradiation time, a limit of about 50% of photoexcitation is obtained, while higher intensities allow this value to be overcome. Table 2 summarises the *T*(LIESST) and $T_{1/2}$ values for all the compounds. In the cases of **X = H** and **X = 3,4-Me$_2$**, the derivative of the LIESST curve shows two minima in correlation with the two-step behaviour observed in the thermal spin transition. For **X = 4-Me**, however, the existence of a small anomaly at around 50 K on *T*-(LIESST) curve corresponds to remaining oxygen contamination even when particular precautions were taken to purge the SQUID cavity.

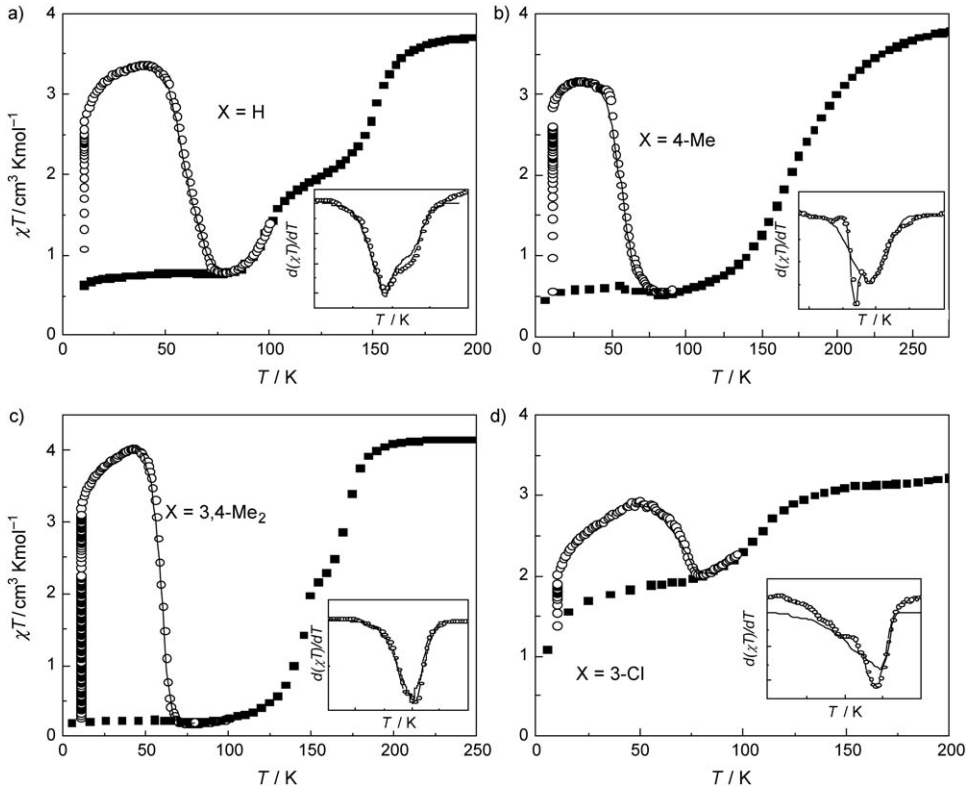

Figure 6. Temperature dependence of χT for Fe(X-py)$_2$[Ag(CN)$_2$)]$_2$. a) **X = H**, b) **X = 4-Me**, c) X = **X = 3,4-Me$_2$** and d) **X = 3-Cl**. ■) Data recorded without irradiation, ○) Irradiation at 10 K and *T*(LIESST) measurement. The inset graphs show the derivatives d(χT)/dT of the LIESST curves as a function of the temperature. The solid lines represent simulations of the LIESST curves.

Table 2. Spin transition and LIESST temperatures of Fe(X-py)$_2$[Ag(CN)$_2$)]$_2$.

X	*T*(LIESST) [K]	$T_{1/2}$ [K]
H	58/65	98/146
3-Me		HS
4-Me	56	ca. 150/ca. 190
3,4-Me$_2$	58/61	145/171
3-Cl	72	109

Relaxation of the light-induced HS state and fitting procedure: The relaxation kinetics of the photoexcited HS state recorded at different temperatures for the four SCO compounds are shown in Figure 7. The experimental procedure consisted of irradiating the sample at 10 K in the SQUID cavity to photoexcite the HS state and heating the sample under continuous irradiation up to the temperature at which the relaxation was to be recorded. Once this temperature is reached and stabilised, the light is turned off and the susceptibility measured as a function of time. From these experiments, one can extract the thermodynamic parameters of the HS–LS conversion process[31] which in turn allow the LIESST curve to be simulated.[4]

In some cases in which the thermal spin transition and the LIESST curve show two steps, the relaxation of the light-induced HS state also reflects this behaviour but, apart from binuclear compounds, few examples have been reported in the literature.[7d,33,34] As in the previously reported compound [Fe(DPEA)(bim)](ClO$_4$)$_2$·0.5 H$_2$O (DPEA = (2-aminoethyl)bis(2-pyridylmethyl)amine, bim = 2,2-bisimidazole),[33] in some of the present cases, a best fit of the relaxation curves was obtained by using a double exponential relaxation, instead of the classical single exponential (low-cooperativity) or sigmoidal (high-cooperativity) decays. Equation (5) describes this double exponential relaxation,

$$\gamma_{HS} = c_1 \exp[-k_{HL1}t] + c_2 \exp[-k_{HL2}t] \quad (5)$$

where c_i ($i = 1, 2$) are the fractions of SCO centres involved in each step (these parameters are fixed in the fit according to the magnetic data), and $k_{HLi}(T)$ are the respective relaxa-

tion process constants. The single stretched exponential decay described by Equation (6) has been used in the other cases. This dependence entails a distribution of the value of the relaxation constant k_{HL} around an average value; β (ranging between 0 and 1) is related to the width of this distribution.[35] The differences between fits using the stretched exponential law and the double exponential law can be appreciated in Figure 7e.

$$\gamma_{HS} = \exp[-(k_{HL}t)^{\beta}] \quad (6)$$

Equation (6) proved to be best suited to fit the decays in the tunnelling regime.

Since k_{HL} can be expressed as Equation (7)[31],

$$k_{HL}(T) = k_{HL(T\to 0)} + k_{HL(T\to\infty)}\exp(-E_a/k_B T) \quad (7)$$

the linear fit of the Arrhenius plot ($\ln k_{HL}$ vs. $1/T$) in the thermally activated region allows calculation of the activation energy E_a and the pre-exponential factor $k_{HL(T\to\infty)}$ for each compound. To a first approximation, for the values of $k_{HL(T\to 0)}$ we consider the relaxation constant corresponding to the lower temperature relaxation among those that reach complete conversion. This can be taken as an upper limit of the $k_{HL(T\to 0)}$ value.[4] The parameters resulting from the fits for all compounds, together with the E_a and $k_{HL(T\to\infty)}$ values deduced from the Arrhenius plots (Figure 7f), are listed in Table 3. These thermodynamic parameters are on the order of those observed in other spin-crossover compounds[31] and, in the cases where a double exponential describes the relaxation (**X=H**, **X=3,4-Me$_2$**), similar to those reported for other polymeric compounds with two-step transitions.[7d]

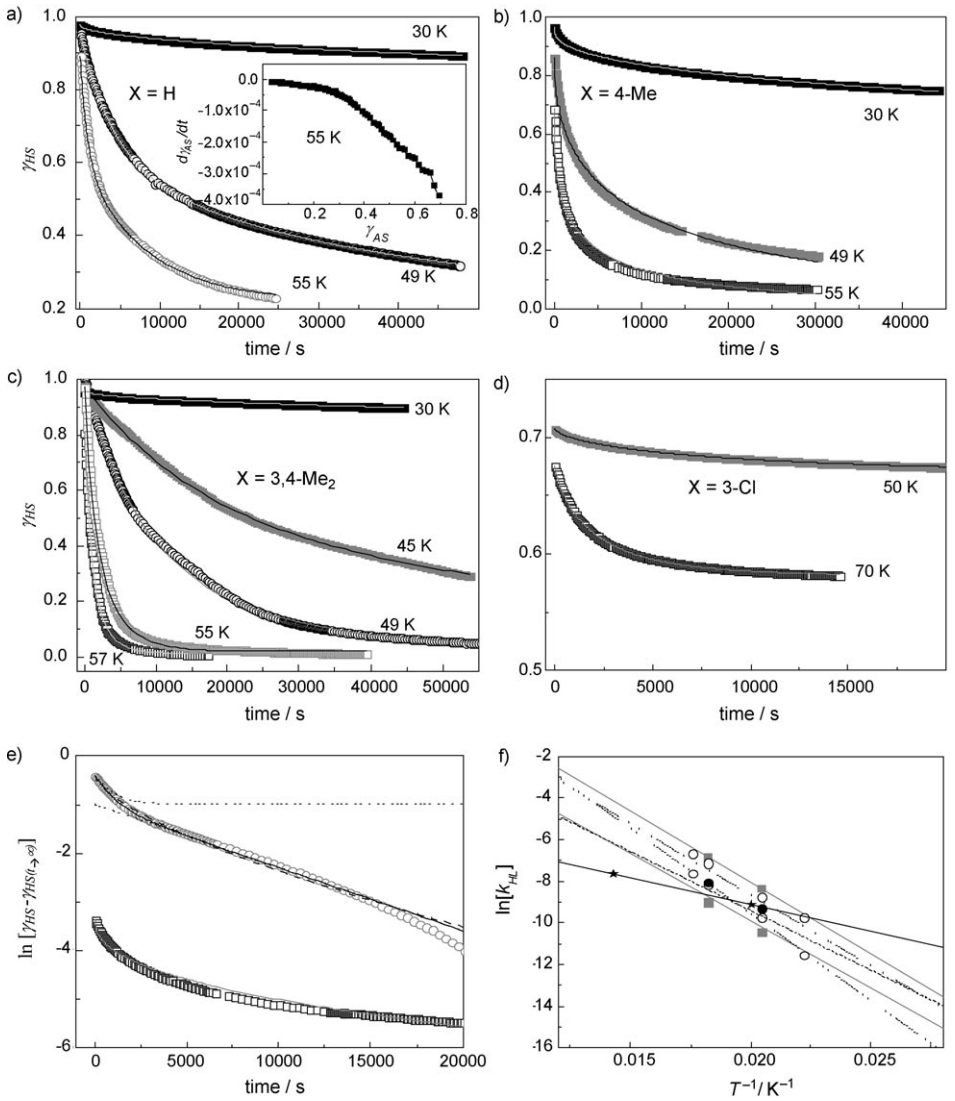

Figure 7. Time dependence of the γ_{HS} fraction (symbols) and fits (continuous lines) at different temperatures for Fe(X-py)$_2$[Ag(CN)$_2$]$_2$. a) **X=H**, b) **X=4-Me**, c) **X=3,4-Me$_2$** and d) **X=3-Cl**. The inset in a) shows $d\gamma_{HS}/dt$ versus t for relaxation at 55 K. e) Logarithmic plot of two selected relaxation curves: **X=H** at 55 K (○), stretched exponential fit (dashed line), double exponential fit (continuous line) and the two exponentials of the latter shown independently (dotted lines); **X=4-Me** at 55 K (□, shifted for clarity) and stretched exponential fit (continuous grey line). f) Arrhenius plot of the k_{HL} constants obtained from the fits of the relaxation curves (symbols) and parameters of the fitting of the LIESST curves (lines): **X=H** (■ and grey solid lines); **X=4-Me** (● and black dashed line); X=**X=3,4-Me$_2$** (○ and black dotted lines); **X=3-Cl** (★ and black solid line).

The relaxation at 30 K for **X=H** (Figure 7a), corresponds to a process occurring in the tunnelling regime: in about 13 h, only about 8% of the light-induced HS fraction has relaxed. On the contrary, the relaxations at 49 and 55 K are almost complete after the same time interval. Although the two-step process is not evident from the relaxation curves, the $d\gamma_{HS}/dt$ versus γ_{HS} plot (inset in Figure 7a) reveals the existence of two relaxation constants. Accordingly, the best fits of both curves are obtained with Equation (5). The thermodynamic parameters were deduced separately for each transition step (Table 3). The behaviour of **X=3,4-Me$_2$** is similar to that observed in compound **X=H**. Even though, taking into account the hysteresis of the low-temperature step, compound **X=H** can be considered a cooperative system, stretched exponential shapes of the relaxation curves are observed in-

Table 3. Thermodynamic parameters for relaxation from the LIESST state.

X	T [K]	k_{HL} [s^{-1}]	c_i	β	E_a [cm^{-1}]	$k_{HL(T\to\infty)}$ [s^{-1}]
H	30	3.2×10^{-7}	–	0.7		
	49	$k_{HL1}=3.0\times10^{-5}$, $k_{HL2}=2.5\times10^{-4}$	$c_1=0.43$, $c_2=0.32$	–	$E_{a1}=476$, $E_{a2}=448$	$k_{HL1(T\to\infty)}=290$, $k_{HL2(T\to\infty)}=15$
	55	$k_{HL1}=1.3\times10^{-4}$, $k_{HL2}=1.1\times10^{-3}$	$r_{HS}=0.23$	–		
4-Me	30	7.9×10^{-7}	–	0.5		
	49	9.3×10^{-5}		0.44	383	7
	55	3.2×10^{-4}		0.42		
3,4-Me_2	30	1.45×10^{-7}	–	0.55		
	45	$k_{HL1}=1.0\times10^{-5}$, $k_{HL2}=6.0\times10^{-5}$	$c_1=0.47$, $c_2=0.53$	–	$E_{a1}=461$, $E_{a2}=566$	$k_{HL1(T\to\infty)}=140$, $k_{HL2(T\to\infty)}=891$
	49	$k_{HL1}=6.0\times10^{-5}$, $k_{HL2}=1.6\times10^{-4}$				
	55	$k_{HL1}=2.9\times10^{-4}$, $k_{HL2}=8.2\times10^{-4}$				
	57	$k_{HL1}=5.0\times10^{-4}$, $k_{HL2}=1.3\times10^{-3}$				
3-Cl	50	1.1×10^{-4}	–	0.7	ca. 178	ca. 0.02
	70	4.8×10^{-4}		0.7		

The calculated curves are shown as solid lines in Figure 6, and the fitting parameters E_a and $k_{HL(T\to\infty)}$ are listed in Table 4 and represented in Figure 7e. In all cases the shape and position of the curves is well described, with fitting parameters close to the values obtained from the Arrhenius plots. The differences between the calculated and experimental curves can be better appreciated in the representation of the derivatives. In **X = 3-Cl**, only T-(LIESST) is well reproduced and not the shape of the derivative, probably due to the lack of precision in the determination of the thermodynamic parameters with only two relaxation curves and, as in **X = 4-Me**, to the existence of a small anomaly at around 50 K corresponding to oxygen contamination. On the other hand, in the case of **X = H**, the agreement is quite satisfactory. For **X = 3,4-Me_2**, the two T(LIESST) are less evident, probably due to the proximity of the two values.

Table 4. Fitting parameters of the LIESST curves.

X	E_a [cm^{-1}]	$k_{HL(T\to\infty)}$ [s^{-1}]
H	$E_{a1}=477$	$k_{HL1(T\to\infty)}=290$
	$E_{a2}=448$	$k_{HL2(T\to\infty)}=20$
4-Me	395	7
3,4-Me_2	$E_{a1}=451$, $E_{a2}=530$	$k_{HL1(T\to\infty)}=190$, $k_{HL2(T\to\infty)}=900$
3-Cl	178	0.02

stead of the expected sigmoidal shape. The stretched exponential shapes are typical of a broad distribution of relaxation times, which are expected to be associated with structural disorders,[36] as observed in this compound.[19]

In the case of the other two compounds that show spin transition, the phenomenon is better described by a stretched exponential equation. For **X = 4-Me**, also the relaxations out of the tunnelling regime are hence best fitted with Equation (6). The two-step process is not evident, as in the magnetic curve of the thermal spin transition. However, the low values of β (0.4–0.5) are compatible with the existence of strongly overlapping bimodal distribution of relaxation constants. Also for **X = 3-Cl**, the relaxation curves have been fitted to stretched exponential decays, as expected for a single relaxation process. In contrast to the other complexes, at 50 K the relaxation affects only 3% of the SCO centres after more than 4 h, and complete relaxation is recorded only at 70 K. This makes the estimation of E_a and $k_{HL(T\to\infty)}$ imprecise.

Simulation of the LIESST curves by using the thermodynamic parameters, as proposed by Létard,[4] was performed to check the overall consistency of the photomagnetic data. The procedure was adapted for two-step processes, for which the LIESST curve is fitted with Equations (8).

$$\left(\frac{\partial\gamma_{HS,i}}{\partial t}\right)_T = -\gamma_{HS,i}\{k_{HL,i(T\to0)} + k_{HL,i(T\to\infty)}\exp[-E_{a,i}/k_BT]\} \quad (i=1,2) \tag{8a}$$

$$\gamma_{HS} = c_1\gamma_{HS,1} + c_2\gamma_{HS,2} \tag{8b}$$

The calculation was performed by considering that the temperature of a given experimental point governs the relaxation in the time interval between that experimental point and the next one.

Only tentative explanations can be given for the origin of the observed two-step behaviour in most of the compounds of the family, because of the above-mentioned lack of precise structural information. Most commonly, the origin of the two-step transition in both mononuclear and polymeric compounds is due to the presence of two or more lattice sites with different SCO transition temperatures. The presence of different sites can happen in the whole temperature range or only in a part of it, induced by a structural transition, but this is not so in our case, at least in the parent compound.[19] In other cases, such as dinuclear systems,[37] the combined effect of elastic antiferromagnetic-like interactions and cooperative ferromagnetic-like intermolecular interactions is responsible for the two-step behaviour. The presence of short range antiferromagnetic-like interactions seems to play a crucial role in this behaviour.[38]

Conclusion

The present work enlarges the series of rare examples of SCO compounds—other than binuclear ones—in which two-

step behaviour is shown not only in the thermal spin transition, but also in the relaxation of the photoinduced HS metastable state. We have investigated, by means of magnetic, photomagnetic, calorimetric, Mössbauer and reflectivity measurements, the thermal SCO phenomenon in a new series of 2D coordination polymers with general formula $Fe(X\text{-}py)_2[Ag(CN)_2)]_2$ (py = pyridine, X = 3-Cl, 3-Me, 4-Me, X = 3,4-Me_2) and their light-induced properties together with the parent compound $Fe(py)_2[Ag(CN)_2)]_2$. Most of the compounds of the family (X = H, 4-Me, 3,4-Me_2) undergo an almost complete two-step spin transition, while for compound **X = 3-Cl** the transition is incomplete, and for **X = 3-Me** the system remains in the HS state in the whole temperature range. The influence of the substituents in the pyridine ligand has been found to be opposite to that expected solely from electronic considerations, and the crystal packing is believed to be the main reason for this behaviour. The thermodynamic parameters associated with the spin transition were obtained from heat capacity measurements, and the consistency of the thermodynamic and magnetic data analysed by using a simple model proposed by Real and co-workers based on the regular solution model of Slichter and Drickamer, which also gives information about the cooperativity of these compounds.

Except for **X = 3-Me**, all of the studied compounds show quantitative LIESST with stretched exponential decays of the light-induced state, symptomatic of a low-cooperativity process. The thermodynamic parameters obtained from the analysis of the relaxation curves were used to calculate the LIESST curves and thus check the consistency of the photomagnetic study. The compounds that show a two-step thermal spin transition interestingly reveal a two-step character also in the relaxation of the photoinduced HS metastable state, which is a quite uncommon feature for this type of compounds.

Experimental Section

Synthesis: The $Fe(X\text{-}py)_2[Ag(CN)_2]_2$ family was prepared by the method applied for $Cd(py)_2[Ag(CN)_2]_2$[39] and $Fe(py)_2[Ag(CN)_2]_2$,[19] but with the corresponding substituted ligand instead of pyridine. Elemental analysis calcd (%) for $Fe(3\text{-}Clpy)_2[Ag(CN)_2]_2$ ($FeC_{14}H_8N_6Cl_2Ag_2$): C 27.90, H 1.33, N 13.95; found: C 27.11, H 1.27, N 13.11. Elemental analysis calcd (%) for $Fe(4\text{-}mepy)_2[Ag(CN)_2]_2$ ($FeC_{16}H_{14}N_6Ag_2$): C 34.20, H 2.49, N 14.96; found: C 34.60, H 2.61, N 14.24. Elemental analysis calcd (%) for $Fe(3\text{-}mepy)_2[Ag(CN)_2]_2$ ($FeC_{16}H_{14}N_6Ag_2$): C 34.20, H 2.49, N 14.96; found: C 34.39, H 2.52, N 14.96. Elemental analysis calcd (%) for $Fe(3,4\text{-}Me_2py)_2[Ag(CN)_2]_2$ ($FeC_{18}H_{18}N_6Ag_2$): C 36.65, H 3.05, N 14.25; found: C 37.20, H 2.93, N 13.93.

Reflectivity: The reflectivity of the samples was measured with a homemade set-up equipped with a CVI spectrometer. This system allows to collect the reflectivity spectra within the range of 450–950 nm at a constant temperature and to follow the temperature dependence of the signal between 5 K and 290 K at a selected wavelength (±2.5 nm). The sample was a thin layer of the powdered compound without any dispersion in a matrix.[35]

Magnetic susceptibility and photomagnetic measurements: The magnetisation versus temperature measurements were performed on a MPMS-XL Quantum Design SQUID magnetometer between 5 and 300 K in an external field of 1 T. A sample mass of about 15 mg was used. The data were corrected for the magnetisation of the sample holder and for diamagnetic contributions, estimated from Pascal's constants.

The photomagnetic measurements were performed with a Spectra Physics Series 2025 Kr^+ laser ($\lambda = 530.9$ nm) coupled by an optical fibre to the cavity of the SQUID magnetometer (MPMS-55 Quantum Design) operating with an external magnetic field of 2 T. The temperature range was 2–300 K and the scan rate 0.3 K min^{-1}. The power at the sample was adjusted to 5 mW cm^{-2}. Bulk attenuation of light intensity was limited as much as possible by preparation of a thin layer of compound. It is noteworthy that there was no change in the data due to heating of the sample upon laser irradiation.

The weight of these thin layer samples (approximately 0.2 mg) was estimated by comparison of their thermal spin-crossover curves with the experimental magnetic data obtained with a more accurately weighted sample of the same compound.

Mössbauer spectroscopy: ^{57}Fe Mössbauer experiments were carried out on cooling from 290 to 78 K on a Wissel Mössbauer spectrometer consisting of an MDU-1200 driving unit and a MVT-100 velocity transducer, incorporating a Seiko Model 7800 multichannel analyzer. The powder samples (ca. 60 mg) were kept in a Heli-Tan LT-3 gas-flow cryostat (Advanced Research System Inc.) equipped with a 9620 digital temperature controller from Scientific Instruments. The $^{57}Co(Rh)$ source was maintained at room temperature.

Calorimetric measurements: Heat capacity was measured in the 100–300 K temperature range with a differential scanning calorimeter (Q1000 model from TA Instruments) at a heating rate of 10 K min^{-1}. Calibration in temperature and energy was performed with a standard sample of indium by using its melting transition (429.76 K, 3.296 kJ mol^{-1}), while for the heat capacity calibration a sapphire sample was used and measured under the same conditions as the studied samples. The measurements were carried on powder samples of about 15 mg. For **X = 3-Cl**, heat capacity was measured by ac calorimetry in the 5–300 K temperature range. In this case, the sample is a pressed disc (3 mm diameter, ca. 100 μm thick, weighting ca. 1 mg). With this technique, only relative heat capacity values are measured, and then absolute values are determined by scaling the data to the results obtained by DSC around room-temperature.

Acknowledgements

This work was supported by the Spanish MICINN and FEDER, projects MAT2007-61621 and CSD2007-00010. The European Union Network of Excellence MAGMANet is also acknowledged.

[1] *Molecular Magnets: Recent Highlights* (Eds.: W. Linert, M. Verdaguer), Springer, Wien, **2003**.
[2] *Spin-Crossover in Transition Metal Compounds, Vols. I & II* (Eds.: P. Gütlich, H. A. Goodwin), Springer, Berlin, **2004**.
[3] S. Decurtins, P. Gütlich, C. P. Kölher, H. Spiering, A. Hauser, *Chem. Phys. Lett.* **1984**, *105*, 1.
[4] J. F. Létard, *J. Mater. Chem.* **2006**, *16*, 2550–2559, and references therein.
[5] P. Gütlich, Y. Garcia, H. A. Goodwin, *Chem. Soc. Rev.* **2000**, *29*, 419.
[6] J. A. Real, A. B. Gaspar, M. C. Muñoz, *Dalton Trans.* **2005**, 2062.
[7] a) G. Dupouy, M. Marchivie, S. Triki, J. Sala-Pala, C. J. Gómez-García, S. Pillet, C. Lecomte, J. F. Létard, *Chem. Commun.* **2009**, 3404–3406; b) S. M. Neville, B. A. Leita, G. J. Halder, C. J. Kepert, B. Moubaraki, J. F. Letard, K. S. Murray, *Chem. Eur. J.* **2008**, *14*, 10123–10133; c) A. Absmeier, M. Bartel, C. Carbonera, G. N. L. Jameson, P. Weinberger, A. Caneschi, K. Mereiter, J. F. Létard, W. Linert, *Chem. Eur. J.* **2006**, *12*, 2235–2243; d) V. Niel, A. Thompson, A. E. Goeta, C. Enachescu, A. Hauser, A. Galet, M. C. Muñoz, J. A.

Real, *Chem. Eur. J.* **2005**, *11*, 2047–2060; e) V. Niel, A. Galet, A. B. Gaspar, M. C. Muñoz, J. A. Real, *Chem. Commun.* **2003**, 1248.
[8] a) Y. Garcia, V. Ksenofontov, P. Gütlich, *Hyperfine Interact.* **2002**, *139/140*, 543; b) S. B. Erenburg, N. V. Bausk, L. G. Lavrenova, L. N. Mazalov, *J. Magn. Magn. Mater.* **2001**, *226*, 1967; c) X. J. Liu, Y. Morimoto, A. Nakamura, T. Hirao, S. Toyazaki, N. Kojima, *J. Phys. Soc. Jpn.* **2001**, *70*, 2521; d) Y. Garcia, V. Ksenofontov, G. Levchenko, G. Schmitt, P. Gütlich, *J. Phys. Chem. B* **2000**, *104*, 5045; e) S. B. Erenburg, N. V. Bausk, L. G. Lavrenova, L. N. Mazalov, *J. Synchr. Rad.* **1999**, *6*, 576; f) K. Nakao, S. Hayami, M. Akita, K. Inoue, *Chem. Lett.* **2008**, *37*, 292–293.
[9] T. Kitazawa, Y. Gomi, M. Takahasi, M. Takeda, M. Enomoto, A. Miyazaki, T. Enoki, *J. Mater. Chem.* **1996**, *6*, 119.
[10] a) T. Kitazawa, Mi. Takahasi, Ma. Takahasi, M. Enomoto, A. Miyazaki, T. Enoki, M. Takeda, *J. Radioanal. Nucl. Chem.* **1999**, *239*, 285; b) T. Kitazawa, M. Eguchi, M. Takeda, *Mol. Cryst. Liq. Cryst.* **2000**, *341*, 527; c) K. Hosoya, T. Kitazawa, M. Takahasi, M. Takeda, J. F. Meunier, G. Molnár, A. Bousseksou, *Phys. Chem. Chem. Phys.* **2003**, *5*, 1682.
[11] G. Molnár, T. Kitazawa, L. Dubrovinsky, J. J. McGarvey, A. Bousseksou, *J. Phys. Condens. Matter* **2004**, *16*, S1129.
[12] G. Molnár, T. Guillon, N. Moussa, L. Rechignat, T. Kitazawa, M. Nardone, A. Bousseksou, *Chem. Phys. Lett.* **2006**, *423*, 152.
[13] A. Galet, M. C. Muñoz, A. B. Gaspar, J. A. Real, *Inorg. Chem.* **2005**, *44*, 8749.
[14] a) A. Galet, M. C. Muñoz, V. Martínez, J. A. Real, *Chem. Commun.* **2004**, 2268; b) A. Galet, V. Niel, M. C. Muñoz, J. A. Real, *J. Am. Chem. Soc.* **2003**, *125*, 14224.
[15] S. Bonhommeau, G. Molnár, A. Galet, A. Zwick, J. A. Real, J. J. McGarvey, A. Bousseksou, *Angew. Chem.* **2005**, *117*, 4137–4141; *Angew. Chem. Int. Ed.* **2005**, *44*, 4069–4073.
[16] V. Niel, J. M. Martínez-Agudo, M. C. Muñoz, A. B. Gaspar, J. A. Real, *Inorg. Chem.* **2001**, *40*, 3838–3839.
[17] G. Agustí, S. Cobo, A. B. Gaspar, G. Molnár, N. O. Moussa, P. A. Szilágyi, V. Pálfi, C. Vieu, M. C. Muñoz, J. A. Real, A. Bousseksou, *Chem. Mater.* **2008**, *20*, 6721–6732.
[18] V. Niel, M. C. Muñoz, A. B. Gaspar, A. Galet, G. Levchenko, J. A. Real, *Chem. Eur. J.* **2002**, *8*, 2446.
[19] J. A. Rodríguez-Velamazán, M. Castro, E. Palacios, R. Burriel, T. Kitazawa, T. Kawasaki, *J. Phys. Chem. B* **2007**, *111*, 1256–1261.
[20] M. C. Muñoz, A. B. Gaspar, A. Galet, J. A. Real, *Inorg. Chem.* **2007**, *46*, 8182–8192.
[21] G. Agustí, M. C. Muñoz, A. B. Gaspar, J. A. Real, *Inorg. Chem.* **2008**, *47*, 2552–2561.
[22] V. Martínez, A. B. Gaspar, M. C. Muñoz, G. V. Bukin, G. Levchenko, J. A. Real, *Chem. Eur. J.* **2009**, *15*, 10960–10971.
[23] a) K. Nakano, N. Suemura, K. Yoneda, S. Kawata, S. Kaizaki, *Dalton Trans.* **2005**, 740; b) J. F. Létard, C. Carbonera, J. A. Real, S. Kawata, S. Kaizaki, *Chem. Eur. J.* **2009**, *15*, 4146–4155.
[24] M. Sorai, *Top. Curr. Chem.* **2004**, *235*, 153.
[25] R. Boča, M. Boča, H. Ehrenberg, H. Fuess, W. Linert, F. Renz, I. Svoboda, *Chem. Phys.* **2003**, *293*, 375.
[26] J. A. Rodríguez-Velamazán, M. Castro, E. Palacios, R. Burriel, J. S. Costa, J. F. Létard, *Chem. Phys. Lett.* **2007**, *435*, 358.
[27] C. P. Slichter, H. G. Drickamer, *J. Chem. Phys.* **1972**, *56*, 2142.
[28] P. Gütlich, H. A. Goodwin, *Top. Curr. Chem.* **2004**, *233*, 1.
[29] K. F. Purcell, M. P. Edwards, *Inorg. Chem.* **1984**, *23*, 2620.
[30] L. Capes, J. F. Létard, O. Kahn, *Chem. Eur. J.* **2000**, *6*, 2246.
[31] A. Hauser, *Top. Curr. Chem.* **2004**, *233*, 49.
[32] J. F. Létard, P. Guionneau, L. Rabardel, J. A. K. Howard, A. E. Goeta, D. Chasseau, O. Kahn, *Inorg. Chem.* **1998**, *37*, 4432.
[33] G. S. Matouzenko, J.-F. Létard, S. Lecocq, A. Bousseksou, L. Capes, L. Salmon, M. Perrin, O. Kahn, A. Collet, *Eur. J. Inorg. Chem.* **2001**, 2935–2945.
[34] B. A. Leita, S. M. Neville, G. J. Halder, B. Moubaraki, C. J. Kepert, J. F. Létard, K. S. Murray, *Inorg. Chem.* **2007**, *46*, 8784–8795.
[35] C. Carbonera, A. Dei, C. Sangregorio, J.-F. Létard, *Chem. Phys. Lett.* **2004**, *396*, 198–201.
[36] V. Mishra, R. Mukherjee, J. Linares, C. Balde, C. Desplanches, J. F. Létard, E. Collet, L. Toupet, M. Castro, F. Varret, *Inorg. Chem.* **2008**, *47*, 7577–7587.
[37] J. A. Real, A. B. Gaspar, M. C. Muñoz, P. Gütlich, V. Ksenofontov, H. Spiering, *Top. Curr. Chem.* **2004**, *233*, 167.
[38] S. Mouri, K. Tanaka, S. Bonhommeau, N. O. Moussa, G. Molnar, A. Bousseksou, *Phys. Rev. B* **2008**, *78*, 174308.
[39] T. Soma, T. Iwamoto, *J. Inclusion Phenom. Mol. Recognit. Chem.* **1996**, *26*, 161.

Received: February 18, 2010
Published online: June 25, 2010

